AIMS Mathematics, 8(1): 61–75.
DOI: 10.3934/math.2023003
Received: 16 August 2022
Revised: 15 September 2022
Accepted: 22 September 2022
Published: 27 September 2022

http://www.aimspress.com/journal/Math

Research article

Designing Meyer wavelet neural networks for the three-species food chain model

Thanasak Mouktonglang[1,2], Zulqurnain Sabir[3,4], Muhammad Asif Zahoor Raja[5], Saira Bhatti[6], Thongchai Botmart[7,*], Wajaree Weera[7] and Chantapish Zamart[7]

[1] Department of Mathematics, Faculty of Science, Chiang Mai University, Chiang Mai, 50200, Thailand
[2] Advanced Research Center for Computational Simulation, Chiang Mai University, Chiang Mai, 50200, Thailand
[3] Department of Mathematical Sciences, United Arab Emirates University, P. O. Box 15551, Al Ain, UAE
[4] Department of Mathematics, Hazara University, Mansehra, Pakistan
[5] Future Technology Research Center, National Yunlin University of Science and Technology, 123 University Road, Section 3, Douliou, Yunlin 64002, Taiwan, R.O.C
[6] Department of Mathematics, COMSATS University Islamabad, Abbottabad Campus, Abbottabad Pakistan
[7] Department of Mathematics, Faculty of Science, Khon Kaen University, Khon Kaen 40002, Thailand

* **Correspondence:** Email: thongbo@kku.ac.th.

Abstract: The current research work is related to present the numerical solutions of three-species food chain model (TS-FCM) by exploiting the strength of Meyer wavelet neural networks (MWNNs) along with the global and local search competencies. The particle swarm optimization technique works as a global operator, while the sequential quadratic programming scheme is applied as a local operator for the TS-FCM. The nonlinear TS-FCM is dependent upon three categories, called consistent of prey populations, specialist predator and top predator. The optimization of an error-based fitness function is presented by using the hybrid computing efficiency of the global and local search schemes, which is designed through the differential form of the designed ordinary differential model and its initial conditions. The proposed results of the TS-FCM are calculated through the stochastic numerical techniques and further comparison is performed by the Adams method to check the exactness of the

scheme. The absolute error in good ranges is performed, which shows the competency of the proposed solver. Moreover, different statistical procedures have also been used to check the reliability of the proposed stochastic procedure along with forty numbers of independent trials and 10 numbers of neurons.

Keywords: Meyer wavelet neural networks; food chain system; Adam scheme; sequential quadratic programming; statistical soundings; particle swarm optimization
Mathematics Subject Classification: 65K10, 92B20

1. Introduction

The two and three kinds of trophic-level study of the systems of the food chain are considered huge significant in recent years. This study is related to present the numerical solutions of three-species food chain model (TS-FCM) by introducing the Meyer wavelet neural networks (MWNNs) along with the competencies of the global and local search algorithms. The particle swarm optimization (PSO) technique works as a global operator, while the sequential quadratic programming (SQP) scheme is applied as a local operator for the TS-FCM. This nonlinear model depends upon the logistic prey P, Lotka–Volterra special predator V as well as top-predator T [1–8]. The generic form of the TS-FCM is given as [9]:

$$\begin{cases} \frac{dP(x)}{dx} = \boldsymbol{\alpha_0 P(x) - \beta_0 P^2(x) - \frac{\lambda_0 P(x) V(x)}{P(x)+\delta_0}, P_0 = I_1,} \\ \frac{dV(x)}{dx} = \boldsymbol{-\alpha_1 V(x) + \frac{\lambda_1 P(x) V(x)}{\delta_1 + P(x)} - \frac{\lambda_2 V(x) T(x)}{V(x)+\delta_2}, \quad V_0 = I_2,} \\ \frac{dT(x)}{dx} = \boldsymbol{\gamma_3 T^2(x) - \frac{\lambda_3 T^2(x)}{V(x)+\delta_3}, \quad T_0 = I_3.} \end{cases} \tag{1}$$

where P_0, V_0 and T_0 are initial population of P, V, and T, respectively. The nonlinear system (1) indicates the TS-FCM, which has been solved by using the numerical and analytical schemes based on the prey population P, that is applied as a single form of the food predator V and the top-predator T. The prey P features with the V species represents the Volterra approach modelling, which is used to reduce the population of predator exponentially when the prey is missed. The T species association along with with the V prey is achieved based on the Leslie–Gower scheme to reduce the population of the predator [10,11]. The descriptions of the TS-FCM is given in the Table 1. A good source of the information for the interested reader related with food chain model can be seen in [12,13].

The aim of this work is to design a stochastic framework based on the MWNNs for presenting the numerical solutions of the TS-FCM. The PSO technique works as a global operator, while the SQP scheme is applied as a local operator to solve the TS-FCM. The numerical stochastic algorithms have been accomplished to solve various stiff models. To mention some of the applications that have been tackled through the stochastic solvers are smoke differential systems [14], fractional models based on the singular differential equations [15,16], dengue virus model [17], singular higher kind of systems [18–20] and periodic boundary value problems [21–23].

Table 1. Detail of the parameter based TS-FCM.

Parameters	Description
$\boldsymbol{\alpha_0}$	Specific growth rate of *P*
$\boldsymbol{\gamma_3}$	Rate of progression of *T*
$\boldsymbol{\delta_2}$	Rate of exclusion of *V* per capita $0.5\lambda_2$
$\boldsymbol{\delta_3}$	Surplus cost in the *T* species to severe inadequacy of the food *V*
$\boldsymbol{\alpha_1}$	*V* rate that is used to decrease the *P* omission
$\boldsymbol{\delta_0, \delta_1}$	Parameters for production conservation of *P*
$\boldsymbol{\beta_0}$	Power of competition using the individuals of species *P*
$\boldsymbol{\lambda_0, \lambda_1, \lambda_2, \lambda_3}$	Achieved maximum performances/capita by lessoning the *P*

The aim of research work is to present the numerical solutions of three-species food chain model (TS-FCM) by exploiting the strength of Meyer wavelet neural networks (MWNNs) along with the global and local search competencies. The particle swarm optimization (PSO) technique works as a global operator, while the sequential quadratic programming (SQP) scheme is applied as a local operator. As the stochastic algorithms have been used to solve many stiff nature models, but none has applied the MWNNs using the optimization based PSO-SQP. The contributions, novelty and advantages of the designed MWNNs optimized with PSO-SQP are presented briefly as follows:

- The stochastic numerical procedure based on the MWNN models is designed first time to solve the TS-FCM numerically.
- The numerical results of the TS-FCM are provided by using modeling knacks of proposed MWNNs together with the competency of hybrid optimization procedures based on PSO-SQP for training/learning of networks.
- The correctness of the approach MWNNs trained with PSO-SQP is observed with very small values of absolute error (AE) from reference numerical outcomes for solving governing relations of TS-FCM
- The authorization, consistency and reliability of the scheme are acknowledged for larger number of runs based different statistical performances to solve the TS-FCM.

The organization of the paper is presented as: The computational procedures of MWNNs using the optimization procedures of PSO-SQP are given in Section 2. Discussions based on the results are described in Section 3. The final remarks are listed in the last Section.

2. Designed MWNNs procedure

In this section, the stochastic MWNNs using the optimization procedures of PSO-SQP is provided to solve the TS-FCM. An objective function is structured based on some necessary steps of PSO-SQP hybridization of GA-ASA is provided also in this section.

2.1. Proposed process

The mathematical representations of TS-FCM with its first order derivatives are presented as:

$$\left[\hat{P}(x), \hat{V}(x), \hat{T}(x)\right] = \begin{bmatrix} \sum_{s=1}^{q} y_{P,s} Q\left(w_{P,s}x + z_{P,s}\right), \sum_{s=1}^{q} y_{V,s} Q\left(w_{V,s}x + z_{V,s}\right), \\ \sum_{s=1}^{q} y_{T,s} Q\left(w_{T,s}x + z_{T,s}\right) \end{bmatrix}, \tag{2}$$

$$\left[\frac{d\hat{P}}{dx},\frac{d\hat{V}}{dx},\frac{d\hat{T}}{dx}\right]=\begin{bmatrix}\sum_{s=1}^{q} y_{P,s}\frac{d}{dx}Q\left(w_{P,s}x+z_{X,s}\right),\sum_{s=1}^{q} y_{V,s}\frac{d}{dx}Q\left(w_{V,s}x+z_{V,s}\right),\\ \sum_{s=1}^{q} y_{T,s}\frac{d}{dx}Q\left(w_{T,s}x+z_{T,s}\right)\end{bmatrix}.$$

An unidentified vector W is defined as:

$W=[W_P,W_V,W_T]$, for $W_P=[y_P,\omega_P,z_P]$, $W_V=[y_V,\omega_V,z_V]$, and $W_T=[y_T,\omega_T,z_T]$, where

$$y_P=\left[y_{P,1},y_{P,2},y_{P,3},\dots,y_{P,q}\right],y_V=\left[y_{V,1},y_{V,2},y_{V,3},\dots,y_{V,q}\right],y_T=\left[y_{T,1},y_{T,2},y_{T,3},\dots,y_{T,q}\right],$$

$$w_P=\left[w_{P,1},w_{P,2},w_{P,3},\dots,w_{P,q}\right],w_V=\left[w_{V,1},w_{V,2},w_{V,3},\dots,w_{V,q}\right],w_T=\left[w_{T,1},w_{T,2},w_{T,3},\dots,w_{T,q}\right],$$

$$z_P=\left[z_{P,1},z_{P,2},z_{P,3},\dots,z_{P,q}\right],z_V=\left[z_{V,1},z_{V,2},z_{V,3},\dots,z_{V,q}\right],z_T=\left[z_{T,1},z_{T,2},z_{T,3},\dots,z_{T,q}\right].$$

An activation kernel using the Meyer wavelet function $Q(x)$ as reported in [24,25] is given as:

$$Q(x)=35x^4-84x^5+70x^6-20x^7. \tag{3}$$

The updated form of the Eq (2) using the above Eq (3) is given as:

$$\left[\hat{P}(x),\hat{V}(x),\hat{T}(x)\right]=\begin{bmatrix}\sum_{s=1}^{q} y_{P,s}\begin{pmatrix}35(w_{P,s}x+z_{P,s})^4-84(w_{P,s}x+z_{P,s})^5+\\70(w_{P,s}x+z_{P,s})^6-20(w_{P,s}x+z_{P,s})^7\end{pmatrix},\\ \sum_{s=1}^{q} y_{V,s}\begin{pmatrix}35(w_{V,s}x+z_{V,s})^4-84(w_{V,s}x+z_{V,s})^5\\+70(w_{V,s}x+z_{V,s})^6-20(w_{V,s}x+z_{V,s})^7\end{pmatrix},\\ \sum_{s=1}^{q} y_{T,s}\begin{pmatrix}35(w_{T,s}x+z_{T,s})^4-84(w_{T,s}x+z_{T,s})^5\\+70(w_{T,s}x+z_{T,s})^6-20(w_{T,s}x+z_{T,s})^7\end{pmatrix}\end{bmatrix}. \tag{4}$$

A fitness function formulation is given as:

$$E_{Fit}=E_{Fit-1}+E_{Fit-2}+E_{Fit-3}+E_{Fit-4}, \tag{5}$$

$$E_{Fit-1}=\frac{1}{N}\sum_{k=1}^{N}\left[\frac{d\hat{p}}{dx}+\alpha_0\hat{P}_k+\beta_0\hat{P}_k^2+\frac{\lambda_0\hat{P}_k\hat{V}_k}{\delta_0+\hat{P}_k}\right]^2, \tag{6}$$

$$E_{Fit-2}=\frac{1}{N}\sum_{k=1}^{N}\left[\frac{d\hat{V}}{dx}+\alpha_1\hat{V}_k-\frac{\lambda_1\hat{P}_k\hat{V}_k}{\delta_1+\hat{P}_k}+\frac{\lambda_2\hat{V}_k\hat{T}_k}{\delta_2+\hat{V}_k}\right]^2, \tag{7}$$

$$E_{Fit-3}=\frac{1}{N}\sum_{k=1}^{N}\left[\frac{d\hat{T}}{dx}-\gamma_3\hat{T}_k^2+\frac{\lambda_3\hat{T}_k^2}{\delta_3+\hat{V}_k}\right]^2, \tag{8}$$

$$E_{Fit-4}=\frac{1}{3}\left[\left(\hat{P}_0-I_1\right)^2+\left(\hat{V}_0-I_2\right)^2+\left(\hat{T}_0-I_3\right)^2\right], \tag{9}$$

here $\hat{P}_k=P(x_k),\hat{V}_k=V(x_k),\hat{T}_j=T(x_k),Nh=1$, and $x_k=kh$. $\hat{P}_k$, $\hat{V}_k$ and $\hat{T}_k$ are the proposed

solutions. The Eqs (5)–(9) are the error functions based on the TS-FCM and the ICs. Figure 1 shows the design of the MWNNs-PSO-SQP for the TS-FCM.

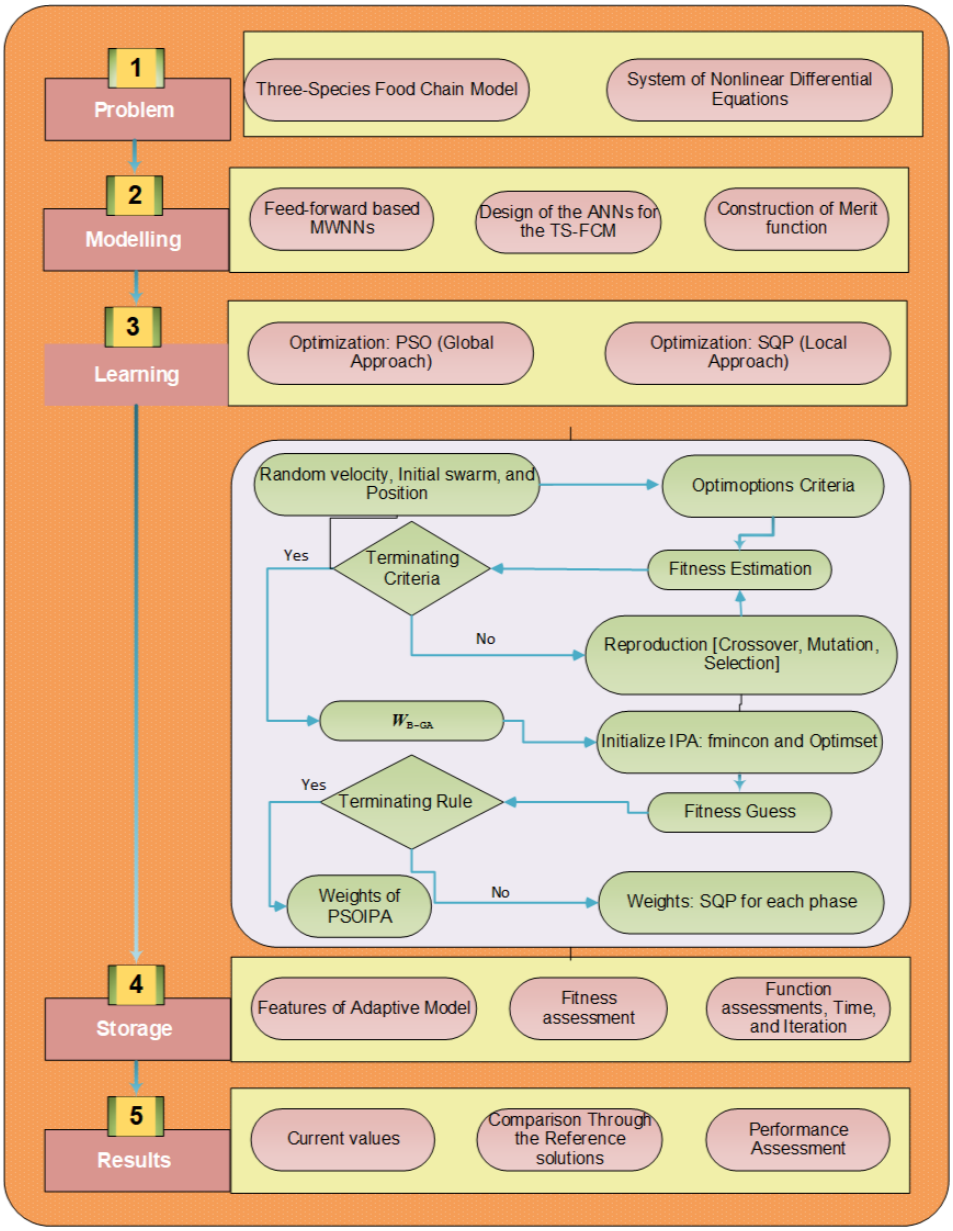

Figure 1. Design of the MWNNs-PSO-SQP for the TS-FCM.

2.2. Network optimization

In this section, the procedures of PSO and SQP are provided.

Particle swarm optimization scheme is one of the global search methods that is used to solve the optimization model and work as an alternate of genetic algorithm (GA). PSO is introduced in the last century as a natural metaheuristic approach because of enormous optimization aptitudes in larger spans of search. PSO performs more efficiently as GA because it has a small memory. In PSO, the prime swarm intensifies in the extensive domain. To improve the parameters of PSO, the system produces

optimal results iteratively that are P_{LB}^{h-1} for the position of swarm and P_{GB}^{h-1} for the velocity of swarm, shown as:

$$\chi_l^h = \chi_l^{h-1} + V_l^{h-1}, \tag{10}$$

$$V_l^h = RV_l^{h-1} - h_1\left(\chi_l^{h-1} - P_{LB}^{h-1}\right)r_1 - h_2\left(\chi_l^{h-1} - P_{GB}^{h-1}\right)r_2, \tag{11}$$

where R, $\boldsymbol{X}_l$ and $\boldsymbol{V}_l$ indicate the weight vector of inertia, position, and velocity, respectively. Whereas acceleration constants are h_1 and h_2. Some prominent submissions of the PSO are classify imbalanced statics [26], features combination to detect the brain tumor [27], diagnosis of breast cancer [28], quality prediction in parts production processes [29], production enhancing based on the biodiesel through Microalga [30] and multilevel thresholding with the subdivision of the health image [31].

PSO converges more reliably with the hybridization of the local SQP, which is applied to assess the adjustment of the results. SQP has been applied in various submissions, some are economic dispatch with non-smooth fuel cost function [32], economic dispatch with valve-point effect [33], power system valve-point economic dispatch problems [34], dynamic dispatch with valve-point effect [35], trajectory optimization [36], kinetic parameters of hydrogenation reactions [37], non-convex short term hydrothermal scheduling problem [38] and equality constrained optimization on Hilbert manifolds [39].

3. Statistical performances

This section narrates the statistical performances using the Theil's inequality coefficient (TIC), semi-interquartile range (SIR) and variance account for (VAF) along with the global depictions for the TS-FCM is given as:

$$[\mathrm{TIC}_P,\mathrm{TIC}_V,\mathrm{TIC}_T] = \left[\begin{array}{c} \frac{\sqrt{\frac{1}{n}\Sigma_{J=1}^{n}\left(P_j-\hat{P}_j\right)^2}}{\left(\sqrt{\frac{1}{n}\Sigma_{J=1}^{n}P_j^2}+\sqrt{\frac{1}{n}\Sigma_{J=1}^{n}\hat{P}_j^2}\right)}, \frac{\sqrt{\frac{1}{n}\Sigma_{J=1}^{n}\left(V_j-\hat{V}_j\right)^2}}{\left(\sqrt{\frac{1}{n}\Sigma_{J=1}^{n}V_j^2}+\sqrt{\frac{1}{n}\Sigma_{J=1}^{n}\hat{V}_j^2}\right)}, \\ \frac{\sqrt{\frac{1}{n}\Sigma_{J=1}^{n}\left(T_j-\hat{T}_j\right)^2}}{\left(\sqrt{\frac{1}{n}\Sigma_{J=1}^{n}T_j^2}+\sqrt{\frac{1}{n}\Sigma_{J=1}^{n}\hat{T}_j^2}\right)} \end{array}\right], \tag{12}$$

$$\mathrm{SIR} = -0.5\left(1^{\mathrm{st}}\mathrm{Quartile} - 3^{\mathrm{rd}}\mathrm{Quartile}\right), \tag{13}$$

$$\begin{cases} [\mathrm{VAF}_P,\mathrm{VAF}_V,\mathrm{VAF}_T] = \left[\begin{array}{c} \left(1-\frac{var\left(P_j-\hat{P}_j\right)}{var\left(P_j\right)}\right)*100, \left(1-\frac{var\left(V_j-\hat{V}_j\right)}{var\left(V_j\right)}\right)*100, \\ \left(1-\frac{var\left(T_j-\hat{T}_j\right)}{var\left(T_j\right)}\right)*100, \end{array}\right] \\ [\mathrm{EVAF}_P,\mathrm{EVAF}_V,\mathrm{EVAF}_T] = [|100-\mathrm{VAF}_P, 100-\mathrm{VAF}_V, 100-\mathrm{VAF}_T|]. \end{cases} \tag{14}$$

where $\hat{P}$, $\hat{V}$ and $\hat{T}$ are the proposed solutions.

4. Results and discussions of the TS-FCM

In this section, the detailed results, and discussions of the TS-FCM based on the stochastic MWNNs-PSO-SQP procedure. The achieved numerical results based TS-FCM have been compared

with the reference solutions to find the correctness of the designed MWNNs-PSO-SQP scheme. The AE plots, the performance of the scheme and convergence routines using VAF, SIR and, TIC operators have been illustrated. The simplified TS-FCM form using the appropriate parameter measures is written as:

$$\begin{cases} \frac{dP(x)}{dx} = 1.5P(x) - 0.06P^2(x) - \frac{P(x)V(x)}{P(x)+10}, P_0 = 1.2, \\ \frac{dV(x)}{dx} = -V(x) + \frac{2P(x)V(x)}{10+P(x)} - \frac{0.405V(x)T(x)}{V(x)+10}, \qquad V_0 = 1.2, \\ \frac{dT(x)}{dx} = 1.5T^2(x) - \frac{\lambda_3 T^2(x)}{V(x)+20}, \qquad T_0 = 1.2. \end{cases} \tag{15}$$

A fitness function using the TS-FCM is given as:

$$E_{Fit} = \frac{1}{N}\sum_{q=1}^{N}\left(\begin{array}{l}\left[\frac{d\hat{p}}{dx} + 1.5\hat{P}_k + 0.06\hat{P}_k^2 + \frac{\hat{P}_k\hat{V}_k}{10+\hat{P}_k}\right]^2 + \left[\frac{d\hat{V}}{dx} + \hat{V}_k - \frac{2\hat{P}_k\hat{V}_k}{10+\hat{P}_k} + \frac{0.0405\hat{V}_k\hat{T}_k}{10+\hat{V}_k}\right]^2 \\ + \left[\frac{d\hat{T}}{dx} - 1.5\hat{T}_k^2 + \frac{\hat{T}_k^2}{20+\hat{V}_k}\right]^2 \end{array}\right) + \frac{1}{3}\left[\left(\hat{P}_0 - 1.2\right)^2 + \left(\hat{V}_0 - 1.2\right)^2 + \left(\hat{T}_0 - 1.2\right)^2\right]. \tag{16}$$

The optimization of the fitness function given in the Eq (16) based on the TS-FCM is performed using the using the proposed MWNNs under the optimization of PSO-SQP procedures. The neurons throughout this work are taken as 10 and the best weight vectors for each class of the TS-FCM is presented in the below equations. The mathematical form of these best weight vectors for each class of the TS-FCM is given as:

$$\begin{aligned}\hat{P}(x) = {} & -3.44(35(-1.7359x + 3.150)^4 - 84(-1.7359x + 3.150)^5 + 70(-1.7359x + 3.150)^6 - \\ & 20(-1.7359x + 3.150)^7) - 1.084(35(-0.2881x + 0.139)^4 - 84(-0.2881x + 0.139)^5 + \\ & 70(-0.2881x + 0.139)^6 - 20(-0.2881x + 0.139)^7) - 0.928(35(-0.518x + 0.0176)^4 - \\ & 84(-0.518x + 0.0176)^5 + 70(-0.518x + 0.0176)^6 20(-0.518x0.0176)^7) + \cdots + \\ & 1.8520(35(0.0016x + 1.9229)^4 - 84(0.0016x + 1.9229)^5 + 70(0.0016x + 1.9229)^6 - \\ & 20(0.0016x + 1.9229)^7),\end{aligned} \tag{17}$$

$$\begin{aligned}\hat{V}(x) = {} & 1.4861(35(-1.900x - 2.2698)^4 - 84(-1.900x - 2.2698)^5 + 70(-1.900x - 2.2698)^6 - \\ & 20(-1.900x - 2.2698)^7) - 0.4707(35(-0.4707x - 1.331)^4 - 84(-0.4707x - 1.331)^5 + \\ & 70(-0.4707x - 1.331)^6 - 20(-0.4707x - 1.331)^7) - 0.1584(35(0.3672x + 0.6896)^4 - \\ & 84(0.3672x + 0.6896)^5 + 70(0.3672x + 0.6896)^6 - 20(0.3672x + 0.6896)^7) + \cdots + \\ & 0.2417(35(0.4986x + 0.6398)^4 - 84(0.4986x + 0.6398)^5 + 70(0.4986x + 0.6398)^6 - \\ & 20(0.4986x + 0.6398)^7),\end{aligned} \tag{18}$$

$$\begin{aligned}\hat{T}(x) = {} & -2.205(35(4.7785x + 2.0850)^4 - 84(4.7785x + 2.0850)^5 + 70(4.7785x + 2.0850)^6 - \\ & 20(4.7785x + 2.0850)^7) - 0.4081(35(0.2606x + 0.4083)^4 - 84(0.2606x + 0.4083)^5 + \\ & 70(0.2606x + 0.4083)^6 - 20(0.2606x + 0.4083)^7) + 1.6674(35(4.0804x + 1.4421)^4 - \\ & 84(4.0804x + 1.4421)^5 + 70(4.0804x + 1.4421)^6 - 20(4.0804x + 1.4421)^7) + \cdots - \\ & 2.5064(35(2.9104x + 1.7957)^4 - 84(2.9104x + 1.7957)^5 + 70(2.9104x + 1.7957)^6 - \\ & 20(2.9104x + 1.7957)^7),\end{aligned} \tag{19}$$

The best values of the weights, comparison performances of the solutions and AE is illustrated in

Figures 1–3 for the TS-FCM using the stochastic numerical schemes. The neurons have been taken as 10 with 30 numbers of variables for solving the TS-FCM. The calculated outcomes using the MWNNs under the optimization of PSO-SQP procedures are drawn in Figures 2(a)–(c) based on the Eqs (17)–(19) for TS-FCM. The comparison performances of the worst, best and mean outcomes is authenticated in Figures 2(d-f) for the TS-FCM. The overlapping of the results indicates that the proposed stochastic scheme for solving the model. The AE plots drawn in Figures 3(a)–(c) for each category of the TS-FCM. These plots indicate best performances based on the mean/best results. It is indicated that the best AE measures for $P(x)$, $V(x)$ and $T(x)$ found as 10^{-06}-10^{-08}, 10^{-05}-10^{-07} and 10^{-05}-10^{-06}, while the mean AE for $P(x)$, $V(x)$ and $T(x)$ found as 10^{-04}-10^{-06}, 10^{-05}-10^{-06} and 10^{-04}-10^{-06}. The performances of the operators EVAF and TIC for TS-FCM are provided in the last portion of Figure 3. For $P(x)$, the EVAF, RMSE and TIC best values found as 10^{-12}-10^{-14}, 10^{-06}-10^{-08} and 10^{-10}-10^{-12}. For $V(x)$, these measures lie as 10^{-10}-10^{-12}, 10^{-06}-10^{-08} and 10^{-10}-10^{-11}. Likewise, for $T(x)$, these gages found as 10^{-10}-10^{-12}, 10^{-05}-10^{-06} and 10^{-10}-10^{-11}. The EVAF and TIC gages together with the plots of histogram based MWNNs under the optimization of PSO-SQP procedures are drawn in Figures 4 and 5. It is seen that most of the independent runs obtained a level of accuracy for the TIC and EVAF gages for solving the TS-FCM.

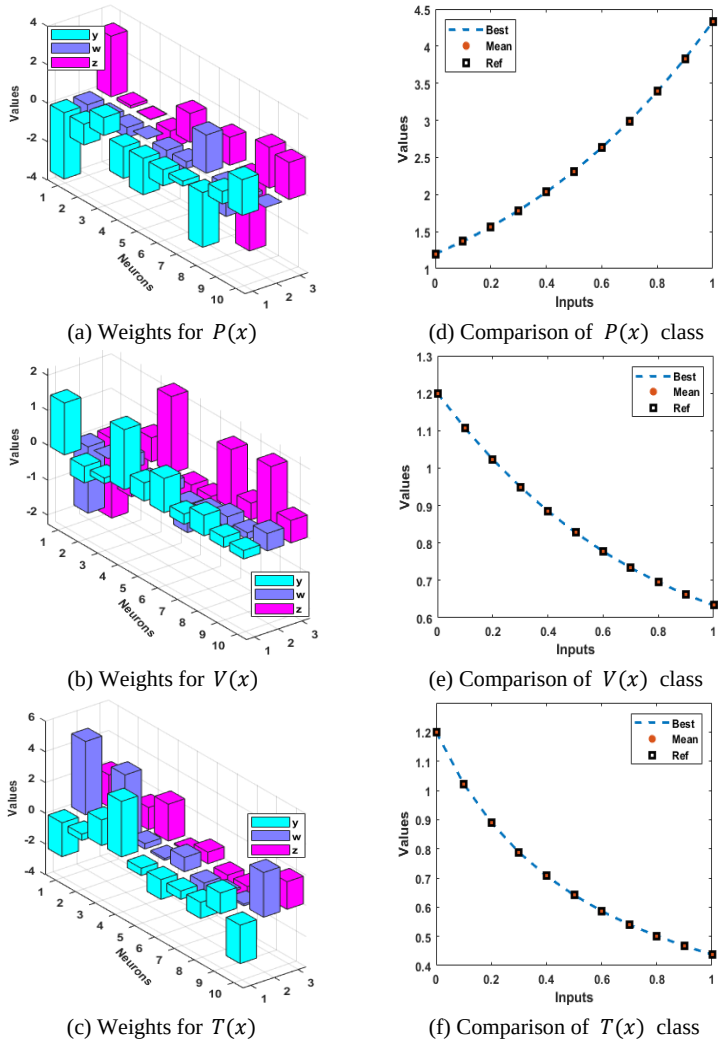

(a) Weights for $P(x)$ (d) Comparison of $P(x)$ class

(b) Weights for $V(x)$ (e) Comparison of $V(x)$ class

(c) Weights for $T(x)$ (f) Comparison of $T(x)$ class

Figure 2. Weights for each class of the TS-FCM (a)–(c) and comparison of the results (d)–(f).

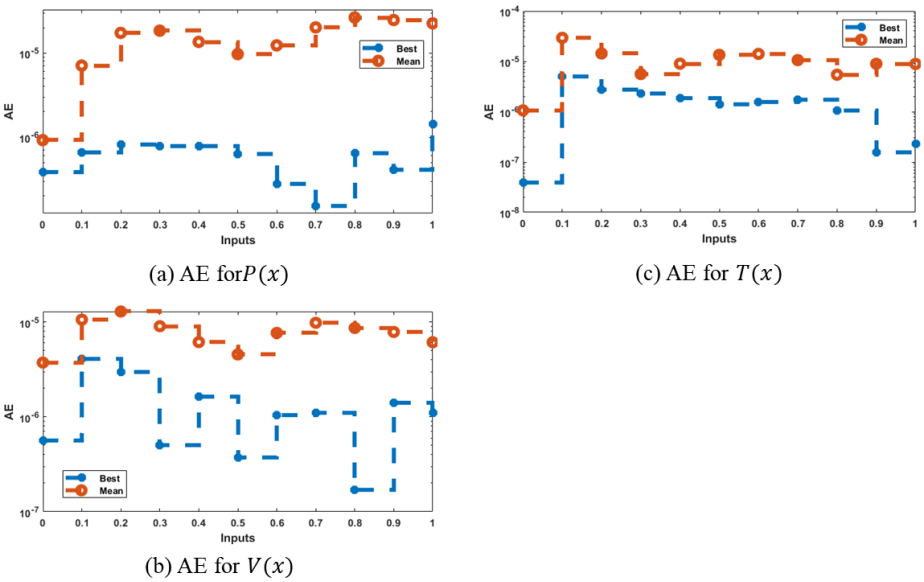

(a) AE for$P(x)$ (c) AE for $T(x)$

(b) AE for $V(x)$

Figure 3. AE and performances of the TIC and EVAF operators for TS-FCM.

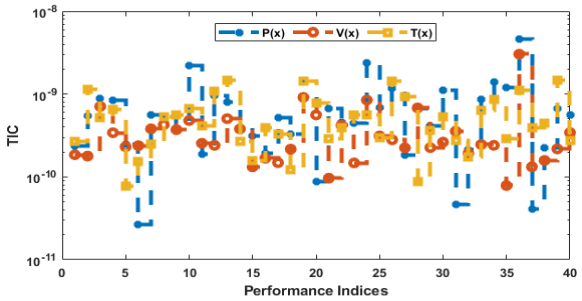

TIC gage performances for the TS-FCM

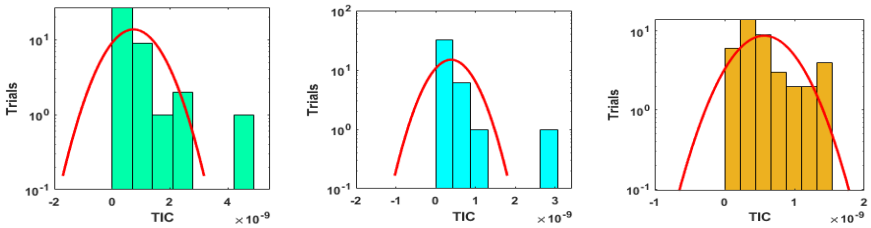

(a) Histogram for $P(x)$ (b) Histogram for $V(x)$ (c) Histogram for $T(x)$

Figure 4. Performances of TIC gages together with histogram based MWNNs-PSO-SQP procedures.

Tables 2 to 4 shows the statistical operator values for each category of the TS-FCM. The statistical values based on the minimum, median, SIR, mean, maximum and standard deviation (S.D) have also been used to analyze the statistical performances of the TS-FCM by using the proposed MWNNs-PSO-SQP approach. The maximum values represent the worst runs and it is observed that the worst runs also found around 10^{-04} to 10^{-05}. While the Minimum performances indicate the good trials, and it is observed that the best runs are calculated as 10^{-07} to 10^{-09}. Moreover, the median, SIR, mean, and S.D values also lie around in good measures that are around 10^{-05} to 10^{-07} for each class of the TS-FCM.

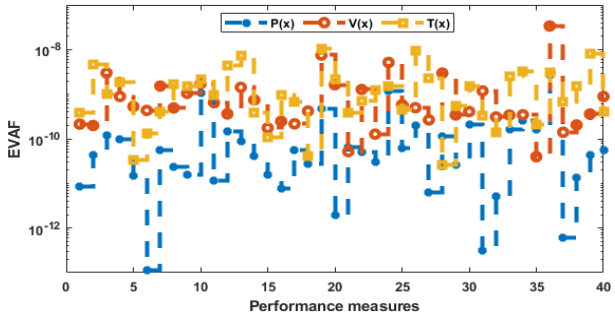

EVAF gage performances for the TS-FCM

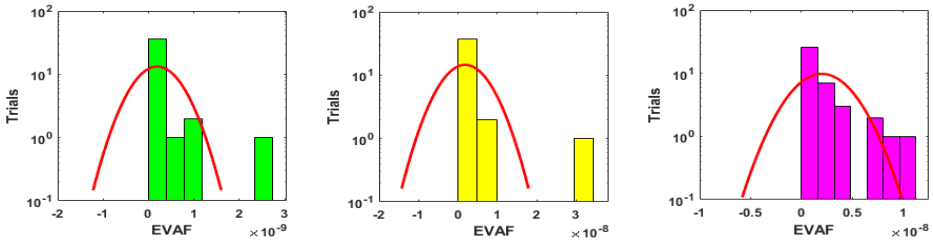

(a) Histogram for $P(x)$ (b) Histogram for $V(x)$ (c) Histogram for $T(x)$

Figure 5. Performances of EVAF gages together with histogram based MWNNs under the optimization of PSO-SQP procedures.

Table 2. Statistical operators for the TS-FCM based $P(x)$ category.

x	$P(x)$					
	Maximum	Minimum	Median	SIR	Mean	S.D
0	1.560E-05	1.306E-09	1.650E-07	2.803E-07	9.229E-07	2.631E-06
0.1	2.770E-05	1.509E-07	4.559E-06	3.795E-06	7.108E-06	6.992E-06
0.2	9.269E-05	5.038E-07	1.259E-05	7.821E-06	1.738E-05	1.969E-05
0.3	1.150E-04	3.931E-07	1.013E-05	9.751E-06	1.849E-05	2.335E-05
0.4	7.951E-05	3.019E-08	8.277E-06	6.633E-06	1.359E-05	1.580E-05
0.5	4.894E-05	4.518E-08	7.653E-06	5.003E-06	9.726E-06	1.013E-05
0.6	5.524E-05	9.898E-09	8.524E-06	6.815E-06	1.236E-05	1.263E-05
0.7	1.175E-04	1.538E-07	1.341E-05	7.795E-06	2.022E-05	2.307E-05
0.8	1.748E-04	3.748E-08	1.608E-05	1.123E-05	2.653E-05	3.456E-05
0.9	1.547E-04	5.977E-08	1.512E-05	1.106E-05	2.473E-05	2.980E-05
1	1.172E-04	9.026E-07	1.593E-05	1.057E-05	2.258E-05	2.325E-05

Table 3. Statistical operators for the TS-FCM based $V(x)$ category.

x	$V(x)$					
	Maximum	Minimum	Median	SIR	Mean	S.D
0	1.091E-04	5.175E-09	2.212E-07	2.803E-07	3.738E-06	1.725E-05
0.1	1.170E-04	7.323E-08	8.129E-06	3.795E-06	1.059E-05	1.781E-05
0.2	4.539E-05	1.594E-06	9.562E-06	7.821E-06	1.291E-05	9.621E-06
0.3	4.880E-05	3.712E-07	4.250E-06	9.751E-06	9.037E-06	1.217E-05
0.4	8.413E-05	9.092E-09	2.378E-06	6.633E-06	6.147E-06	1.379E-05
0.5	7.417E-05	2.679E-08	2.149E-06	5.003E-06	4.553E-06	1.158E-05
0.6	3.275E-05	1.422E-07	5.479E-06	6.815E-06	7.681E-06	7.202E-06
0.7	2.674E-05	8.017E-08	8.815E-06	7.795E-06	9.818E-06	6.380E-06
0.8	6.019E-05	1.700E-07	6.708E-06	1.123E-05	8.661E-06	9.564E-06
0.9	6.621E-05	2.207E-07	2.778E-06	1.106E-05	7.858E-06	1.241E-05
1	2.633E-05	4.242E-08	2.952E-06	1.057E-05	6.118E-06	7.030E-06

Table 4. Statistical operators for the TS-FCM based $T(x)$ category.

x	$T(x)$					
	Maximum	Minimum	Median	SIR	Mean	S.D
0	1.482E-05	1.405E-09	1.954E-07	2.803E-07	1.062E-06	2.705E-06
0.1	8.653E-05	2.383E-06	2.613E-05	3.795E-06	2.933E-05	2.024E-05
0.2	5.367E-05	1.118E-06	8.362E-06	7.821E-06	1.434E-05	1.227E-05
0.3	4.237E-05	1.899E-08	2.918E-06	9.751E-06	5.597E-06	8.230E-06
0.4	5.365E-05	5.482E-08	7.215E-06	6.633E-06	8.984E-06	9.045E-06
0.5	3.816E-05	1.107E-06	1.267E-05	5.003E-06	1.347E-05	8.201E-06
0.6	5.675E-05	8.576E-07	7.775E-06	6.815E-06	1.407E-05	1.487E-05
0.7	5.195E-05	5.877E-07	3.459E-06	7.795E-06	1.060E-05	1.396E-05
0.8	2.496E-05	7.648E-08	3.311E-06	1.123E-05	5.428E-06	5.716E-06
0.9	4.198E-05	1.746E-08	4.990E-06	1.106E-05	8.954E-06	1.038E-05
1	3.761E-05	2.332E-07	6.006E-06	1.057E-05	8.896E-06	8.509E-06

The obtained good global RMSE, EVAF and TIC operator performances for the TS-FCM are described in Table 5 using forty numbers of independent executions based on the MWNNs under the PSO-SQP optimization procedures. The global Median operator are found as 10^{-05}-10^{-06}, 10^{-09}-10^{-10}, and 10^{-10}-10^{-11} for RMSE, TIC and EVAF. While the global SIR is calculated as 10^{-06}-10^{-07}, 10^{-09}-10^{-10} and 10^{-10}-10^{-11} for the TS-FCM. The optimal close measures via global presentations validate the precision and precision of the MWNNs under the optimization of PSO-SQP procedures.

Table 5. Global representations for the TS-FCM.

Index	G. RMSE		G. TIC		G. EVAF	
	Median	SIR	Median	SIR	Median	SIR
$P(x)$	1.3218E-05	8.0860E-06	5.3079E-10	3.1485E-10	4.6702E-11	6.0644E-11
$V(x)$	6.5471E-06	2.6698E-07	2.5025E-09	1.0578E-09	4.6200E-10	4.8615E-10
$T(x)$	1.1708E-05	5.5292E-06	4.3169E-10	2.2095E-10	9.9967E-10	9.1617E-10

5. Conclusions

The current investigations are related to examine the numerical simulations of nonlinear three-species food chain system by exploiting the strength of Meyer wavelet neural networks along with the global and local search competencies. Few concluding remarks are presented as:

- The stochastic numerical procedure using the MWNNs is presented first time for the TS-FCM numerically.
- The correctness of the MWNNs-PSO-SQP is authenticated via the overlapping of the proposed and reference results.
- The AE measures is calculated in good performances for each class of the TS-FCM, i.e., 10^{-06}-10^{-08}.
- The reliability of the stochastic MWNNs-PSO-SQP approach is approved by taking a large number of trials for the TS-FCM.
- The statistical TIC and EVAF operators have been used to check the convergence of the MWNNs-PSO-SQP approach.
- The minimum, median, SIR, mean, maximum and standard deviation have also been used to analyze the statistical performances of the TS-FCM by using the proposed MWNNs-PSO-SQP approach.
- The global representations are presented based on the median and SIR operators for solving the TS-FCM.

In future, the designed MWNNs trained/learned with PSO-SQP scheme should be implemented to solve patchy model [40], stage-structured models [41], and longer food chain systems [42] as well as other stiff nonlinear systems.

Acknowledgments

The research is partially supported by Chiang Mai University. This research received funding support from the NSRF via the Program Management Unit for Human Resources and Institutional Development, Research and Innovation (Grant number B05F650018).

Conflict of interest

The authors declare that there is no conflict of interests regarding the publication of this paper.

References

1. H. M. El-Owaidy, A. A. Ragab, M. Ismail, Mathematical analysis of a food-web model, *Appl. Math. Comput.*, **121** (2001), 155–167. https://doi.org/10.1016/S0096-3003(99)00269-6
2. Y. A. Kuznetsov, S. Rinaldi, Remarks on food chain dynamics, *Math. Biosci.*, **134** (1996), 1–33. https://doi.org/10.1016/0025-5564(95)00104-2
3. F. Wang, M. N. Khan, I. Ahmad, H. Ahmad, H. Abu-Zinadah, Y. M. Chu, Numerical solution of traveling waves in chemical kinetics: time-fractional Fishers equations, *Fractals*, **30** (2022), 2240051. https://doi.org/10.1142/S0218348X22400515

4. H. I. Freedman, J. H. So, Global stability and persistence of simple food chains, *Math. Biosci.*, **76** (1985), 69–86. https://doi.org/10.1016/0025-5564(85)90047-1
5. H. I. Freedman, P. Waltman, Mathematical analysis of some three-species food-chain models, *Math. Biosci.*, **33** (1977), 257–276. https://doi.org/10.1016/0025-5564(77)90142-0
6. Z. Sabir, Stochastic numerical investigations for nonlinear three-species food chain system, *Int. J. Biomath.*, **15** (2021), 2250005. https://doi.org/10.1142/S179352452250005X
7. S. Muratori, S. Rinaldi, Low-and high-frequency oscillations in three-dimensional food chain systems, *SIAM J. Appl. Math.*, **52** (1992), 1688–1706. https://doi.org/10.1137/0152097
8. M. Umar, Z. Sabir, M. A. Z. Raja, Intelligent computing for numerical treatment of nonlinear prey–predator models, *Appl. Soft Comput.*, **80** (2019), 506–524. https://doi.org/10.1016/j.asoc.2019.04.022
9. Z. Sabir, Stochastic numerical investigations for nonlinear three-species food chain system, *Int. J. Biomath.*, **15** (2022), 2250005. https://doi.org/10.1142/S179352452250005X
10. P. H. Leslie, J. C. Gower, The properties of a stochastic model for the predator-prey type of interaction between two species, *Biometrika*, **47** (1960), 219–234. https://doi.org/10.2307/2333294
11. R. K. Upadhyay, S. R. K. Iyengar, V. Rai, Chaos: An ecological reality? *Int. J. Bifurcat. Chaos*, **8** (1998), 1325–1333. https://doi.org/10.1142/S0218127498001029
12. A. Hastings, T. Powell, Chaos in a three-species food chain, *Ecology*, **72** (1991), 896–903. https://doi.org/10.2307/1940591
13. H. Y. Jin, Z. A. Wang, L. Wu, Global dynamics of a three-species spatial food chain model, *J. Differ. Equ.*, **333** (2022), 144–183. https://doi.org/10.1016/j.jde.2022.06.007
14. Z. Sabir, M. A. Z. Raja, A. S. Alnahdi, M. B. Jeelani, M. A. Abdelkawy, Numerical investigations of the nonlinear smoke model using the Gudermannian neural networks, *Math. Biosci. Eng.*, **19** (2022), 351–370. https://doi.org/10.3934/mbe.2022018
15. Z. Sabir, M. A. Z. Raja, J. L. G. Guirao, M. Shoaib, A novel design of fractional Meyer wavelet neural networks with application to the nonlinear singular fractional Lane-Emden systems, *Alex. Eng. J.*, **60** (2021), 2641–2659. https://doi.org/10.1016/j.aej.2021.01.004
16. Z. Sabir, M. A. Z. Raja, D. Baleanu, Fractional Mayer Neuro-swarm heuristic solver for multi-fractional Order doubly singular model based on Lane-Emden equation, *Fractals*, **29** (2021), 2140017. https://doi.org/10.1142/S0218348X2140017X
17. M. Umar, Z. Sabir, M. A. Z. Raja, Y. G. Sánchez, A stochastic numerical computing heuristic of SIR nonlinear model based on dengue fever, *Results Phys.*, **19** (2020), 103585. https://doi.org/10.1016/j.rinp.2020.103585
18. Z. Sabir, S. Saoud, M. A. Z. Raja, H. A. Wahab, A. Arbi, Heuristic computing technique for numerical solutions of nonlinear fourth order Emden–Fowler equation, *Math. Comput. Simulat.*, **178** (2020), 534–548. https://doi.org/10.1016/j.matcom.2020.06.021
19. Z. Sabir, M. A. Z. Raja, J. L. G. Guirao, M. Shoaib, Integrated intelligent computing with neuro-swarming solver for multi-singular fourth-order nonlinear Emden–Fowler equation, *Comput. Appl. Math.*, **39** (2020), 307. https://doi.org/10.1007/s40314-020-01330-4
20. Z. Sabir, M. A. Z. Raja, M. Umar, M. Shoaib, Design of neuro-swarming-based heuristics to solve the third-order nonlinear multi-singular Emden–Fowler equation, *Eur. Phys. J. Plus*, **135** (2020), 410. https://doi.org/10.1140/epjp/s13360-020-00424-6

21. Z. Sabir, M. A. Z. Raja, J. L. G. Guirao, M. Shoaib, A neuro-swarming intelligence-based computing for second order singular periodic non-linear boundary value problems, *Front. Phys.*, **8** (2020), 224. https://doi.org/10.3389/fphy.2020.00224
22. Y. Che, M. Y. A. Keir, Study on the training model of football movement trajectory drop point based on fractional differential equation, *Appl. Math. Nonlinear Sci.*, **7** (2022), 425–430. https://doi.org/10.2478/amns.2021.2.00095
23. Z. Sabir, C. M. Khalique, M. A. Z. Raja, D. Baleanu, Evolutionary computing for nonlinear singular boundary value problems using neural network, genetic algorithm and active-set algorithm, *Eur. Phys. J. Plus*, **136** (2021), 195. https://doi.org/10.1140/epjp/s13360-021-01171-y
24. Z. Sabir, M. A. Z. Raja, J. L. G. Guirao, T. Saeed, Meyer wavelet neural networks to solve a novel design of fractional order pantograph Lane-Emden differential model, *Chaos Soliton. Fract.*, **152** (2021), 111404. https://doi.org/10.1016/j.chaos.2021.111404
25. Z. Sabir, M. A. Z. Raja, M. Umar, M. Shoaib, D. Baleanu, FMNSICS: Fractional Meyer neuro-swarm intelligent computing solver for nonlinear fractional Lane–Emden systems, *Neural Comput. Appl*, **34** (2022), 4193–4206. https://doi.org/10.1007/s00521-021-06452-2
26. J. Li, Y. Wu, S. Fong, A. J. Tallón-Ballesteros, X. S. Yang, S. Mohammed, et al., A binary PSO-based ensemble under-sampling model for rebalancing imbalanced training data, *J. Supercomput.*, **78** (2022), 7428–7463. https://doi.org/10.1007/s11227-021-04177-6
27. M. Sharif, J. Amin, M. Raza, M. Yasmin, S. C. Satapathy, An integrated design of particle swarm optimization (PSO) with fusion of features for detection of brain tumor, *Pattern Recogn. Lett.*, **129** (2020), 150–157. https://doi.org/10.1016/j.patrec.2019.11.017
28. S. Shahbeig, M. S. Helfroush, A. Rahideh, A fuzzy multi-objective hybrid TLBO–PSO approach to select the associated genes with breast cancer, *Signal Process.*, **131** (2017), 58–65. https://doi.org/10.1016/j.sigpro.2016.07.035
29. Y. Su, L. Han, J. Wang, H. Wang, Quantum-behaved RS-PSO-LSSVM method for quality prediction in parts production processes, *Concurr. Comput. Pract. Exp.*, **34** (2022), e5522. https://doi.org/10.1002/cpe.5522
30. M. A. Abdelkareem, H. Rezk, E. T. Sayed, A. Alaswad, A. M. Nassef, A. G. Olabi, Data on fuzzy logic based-modelling and optimization of recovered lipid from microalgae, *Data Brief*, **28** (2020), 104931. https://doi.org/10.1016/j.dib.2019.104931
31. M. Maitra, A. Chatterjee, A hybrid cooperative–comprehensive learning based PSO algorithm for image segmentation using multilevel thresholding, *Expert Syst. Appl.*, **34** (2008), 1341–1350. https://doi.org/10.1016/j.eswa.2007.01.002
32. P. Attaviriyanupap, H. Kita, E. Tanaka, J. Hasegawa, A hybrid EP and SQP for dynamic economic dispatch with nonsmooth fuel cost function, *IEEE T. Power Syst.*, **17** (2002), 411–416. https://doi.org/10.1109/TPWRS.2002.1007911
33. T. A. A. Victoire, A. E. Jeyakumar, Hybrid PSO–SQP for economic dispatch with valve-point effect, *Electr. Pow. Syst. Res.*, **71** (2004), 51–59. https://doi.org/10.1016/j.epsr.2003.12.017
34. J. S. Alsumait, J. K. Sykulski, A. K. Al-Othman, A hybrid GA–PS–SQP method to solve power system valve-point economic dispatch problems, *Appl. Energ.*, **87** (2010), 1773–1781. https://doi.org/10.1016/j.apenergy.2009.10.007
35. T. A. A. Victoire, A. E. Jeyakumar, A modified hybrid EP–SQP approach for dynamic dispatch with valve-point effect, *Int. J. Elec. Power*, **27** (2005), 594–601. https://doi.org/10.1016/j.ijepes.2005.06.006

36. P. E. Gill, W. Murray, M. A. Saunders, Large-scale SQP methods and their application in trajectory optimization, In: *Computational optimal control*, Switzerland: Birkhäuser Basel, 1994, 29–42. https://doi.org/10.1007/978-3-0348-8497-6_3
37. B. Mansoornejad, N. Mostoufi, F. Jalali-Farahani, A hybrid GA–SQP optimization technique for determination of kinetic parameters of hydrogenation reactions, *Comput. Chem. Eng.*, **32** (2008), 1447–1455. https://doi.org/10.1016/j.compchemeng.2007.06.018
38. S. Sivasubramani, K. S. Swarup, Hybrid DE–SQP algorithm for non-convex short term hydrothermal scheduling problem, *Energ. Convers. Manage.*, **52** (2011), 757–761. https://doi.org/10.1016/j.enconman.2010.07.056
39. A. Schiela, J. Ortiz, An SQP method for equality constrained optimization on Hilbert manifolds, *SIAM J. Optim.*, **31** (2021), 2255–2284. https://doi.org/10.1137/20M1341325
40. N. Bajeux, B. Ghosh, Stability switching and hydra effect in a predator–prey metapopulation model, *Biosystems*, **198** (2020), 104255. https://doi.org/10.1016/j.biosystems.2020.104255
41. B. Ghosh, O. L. Zhdanova, B. Barman, E. Y. Frisman, Dynamics of stage-structure predator-prey systems under density-dependent effect and mortality, *Ecol. Complex.*, **41** (2020), 100812. https://doi.org/10.1016/j.ecocom.2020.100812
42. D. Pal, B. Ghosh, T. K. Kar, Hydra effects in stable food chain models, *Biosystems*, **185** (2019), 104018. https://doi.org/10.1016/j.biosystems.2019.104018

AIMS Press